Selectively Addressing Plasmonic Modes and Excitonic States in a Nanocavity Hosting a Quantum Emitter

Alberto Martín-Jiménez, Óscar Jover, Koen Lauwaet, Daniel Granados, Rodolfo Miranda, and Roberto Otero*

ACCESS | Metrics & More | Article Recommendations | Supporting Information

ABSTRACT: Controlling the interaction between the excitonic states of a quantum emitter and the plasmonic modes of a nanocavity is key for the development of quantum information processing devices. In this Letter we demonstrate that the tunnel electroluminescence of electrically insulated C_{60} nanocrystals enclosed in the plasmonic nanocavity at the junction of a scanning tunneling microscope can be switched from a broad emission spectrum, revealing the plasmonic modes of the cavity, to a narrow band emission, displaying only the excitonic states of the C_{60} molecules by changing the bias voltage applied to the junction. Interestingly, excitonic emission dominates the spectra in the high-voltage region in which the simultaneously acquired inelastic rate is low, demonstrating that the excitons cannot be created by an inelastic tunnel process. These results point toward new possible mechanisms for tunnel electroluminescence of quantum emitters and offer new avenues to develop electrically tunable nanoscale light sources.

KEYWORDS: *tunnel electroluminescence, plasmonic nanocavities, excitons, STM*
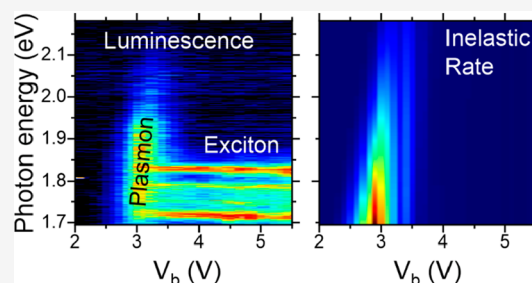
The radiation from systems composed of a quantum emitter (QE) and a nanocavity depends on the strength of the light−matter coupling, leading to Purcell enhancement for weak coupling to the existence of polaritonic modes in the strong coupling regime.[1,2,21] To control and understand the transition between both regimes, it would be convenient to address the plasmonic and excitonic modes separately within the same system. Such a goal is, however, difficult to achieve with conventional optical spectroscopies because the incoming radiation interacts with both cavity modes and QE optical transitions due to its diffraction-limited spatial resolution. A related information can be retrieved by studying the cavity modes of the empty cavity and the excitonic states of the QE outside of the cavity,[3] but this ignores the possible modification in QE and cavity properties when they are brought together.

Scanning tunneling luminescence investigations can potentially open a new way to study QE−cavity interactions in systems consisting of organic molecules separated from metallic surfaces by an atomically thin insulating film.[4−18] The space between the metal surface and the metallic tip can be considered as a tunable plasmonic nanocavity, whose broad optical modes can be studied by collecting tunnel electroluminescence spectra in molecule-free areas.[9,10,13] On the other hand, the electroluminescence spectra recorded on top of the molecules display narrow features that can be attributed to the recombination of molecular excitons.[4−15] The excitation of the plasmonic modes by STM has long been understood as the

result of inelastic tunneling processes,[19,20] but the situation is not so clear for the excitonic case: while many previous studies also consider that such excitation is caused by inelastic events during the tunnel process (via an intermediate plasmon or not),[5−7,10,13] other reports explain the exciton formation as the result of two correlated elastic tunneling processes.[4,14,15] Notice that if the mechanisms for plasmon and exciton creation were different, one might conceive of ways to excite only the plasmonic or only the excitonic modes of the QE +cavity system, offering unique insights into the physics of light−matter interactions at the nanoscale and providing us with a new tool to design color-tunable nanoscale light sources. One attempt in this direction was recently published for the case of multilayer C_{60} on Ag(111), where the current-induced limitation of the exciton lifetime enabled a progressive transformation of excitonic spectra into plasmonic spectra with increasing tunnel current.[14]

In this paper, we demonstrate that the mechanisms for excitonic and plasmonic tunnel electroluminescence in C_{60} nanoislands separated from a Ag(111) surface by a thin (2−3 ML) NaCl film are indeed different, enabling us to address

only the plasmonic or only the excitonic modes of the system by a suitable change of the bias voltage of just about 0.5 V. Our study is based on the simultaneous recording of light intensities and the rate of inelastic excitations for different voltages and photon energies.[21] We show that for the relatively narrow window of bias voltages for which the rate of inelastic transitions is sizable, electroluminescence spectra display a broad emission shape (FWHM $\sim$ 200 meV), ascribed to the plasmonic resonances of the nanocavity, as expected for inelastic excitations.[19,20] On the contrary, for higher voltages with low inelastic rates, excitonic emission, equivalent to that found in single-crystal C_{60}[22] sets in and dominates the spectra up to the maximum measured voltages (about 5.5 V). This fact implies that the energy transfer from the tunneling electron to the exciton cannot occur during the tunneling process. Moreover, the small separation from the LUMO level to the Femi level of Ag(111) also renders implausible the traditional two-tunnel events mechanism. In view of these results, we propose a new mechanism in which a hot electron in a C_{60} molecule injected by an elastic tunnel event relaxes through scattering processes that promote the molecule from the ground state to the excited state, creating the exciton which subsequently decays by the emission of a photon. Our results, thus, shed new light on the mechanisms for excitonic light emission induced by tunnel currents and open the fascinating possibility of choosing the excitation channel for light emission in systems composed of a QE and a nanocavity, which can be exploited for the fabrication of tunable light sources in the nanoscale.

Figure 1 shows the typical morphology of a C_{60} nanocrystal supported on a thin NaCl film grown on Ag(111). The nanocrystals had characteristic truncated triangular shapes with an average lateral size of $\sim$50 nm, with straight edges, and an apparent height of $\sim$2 nm, which corresponds to a vertical stacking of two layers of C_{60} fullerenes.[17,18,23] Figure 1b shows a magnified view of the surface of the nanocrystal of (a), displaying hexagonal self-assembly, with a nearest-neighbor distance between molecules of 0.95 Å. Depending on the absorption configuration, the C_{60} molecules displayed one-, two-, or three-lobed structures.[23]

dI/dV curves recorded on the C_{60} islands (Figure 1c) show two significant features above the Fermi level at about 0.7 and 2.1 eV, respectively, which we attribute to the LUMO and LUMO+1 orbitals. The exact position of these peaks depends on the tunneling conditions due to the insulating nature of the NaCl spacer and the underlying layer of C_{60} molecules.[24] The presence of this insulating film implies that a fraction α of the applied voltage between the tip and the Ag(111) substrate falls between the crystallite surface and the NaCl/Ag interface, α being the ratio between the total capacitance of the junction and the capacitance of the insulating film (see the Supporting Information for more details). The Fermi level and all the molecular orbitals of the C_{60} molecules at the surface of the nanocrystallites would thus be shifted by αeV_B with respect to the Fermi level of the Ag(111) substrate. Thus, the voltages at which the dI/dV peaks appear ($V_{B,i}$) will be related to the energies of the molecular orbitals at zero bias (E_i) by $eV_{B,i} = E_i + \alpha eV_{B,i}$ (see Figure 1d) or $eV_{B,i} = E_i/(1 - \alpha)$. Changes in the tunneling conditions lead to modifications in the total capacitance of the junction and α which, in turn, changes the voltages at which the peaks appear in the dI/dV curves, as observed in Figure 1c. Notice, however, that in the range of tunneling parameters explored here the shifts are small,
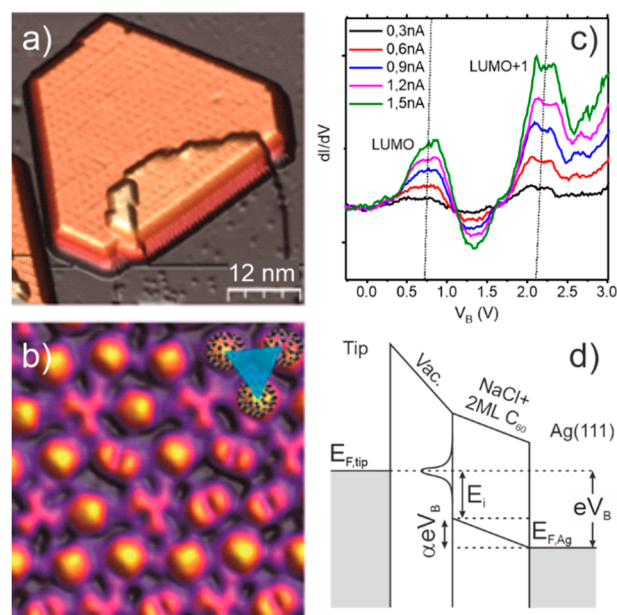
Figure 1. (a) STM topography image of a 2 ML height C_{60} nanocrystal partially nucleated on top of 2 and 3 ML of NaCl (2.5 V; 30 pA; 60 nm $\times$ 60 nm). (b) Molecular self-assembly of the topmost layer of the nanocrystal shown in (b) (1.5 V; 60 pA; 10 nm $\times$ 7 nm). Each molecular structure corresponds to a different adsorption geometry of the C_{60} molecules. (c) dI/dV spectra recorded with different stabilization current set points. The LUMO and LUMO+1 orbitals are clearly visible in these spectra, but their voltage position depends on the tunneling conditions. (d) Schematic diagram illustrating the relation between the applied bias voltage for the peak corresponding to a molecular orbital, the voltage drop between the surface of the crystallite and the NaCl interface, and the position of the molecular orbital with respect to its local electron chemical potential.

implying that α is almost constant. We can obtain an estimation for α by comparing the energy separation between the LUMO and LUMO+1 orbitals in bulk C_{60} obtained by inverse photoemission[25] and in our experiments, yielding a value of about $\alpha = 1 - \Delta E_{IPS}/\Delta V_{STM} = 0.23$. We do not observe any spectral feature at negative voltages which could be attributed to the HOMO orbital because the LUMO orbital is dragged by the action of the negative voltage below the Fermi level of the sample before the HOMO level can be reached (see the Supporting Information for further details).

Tunnel electroluminescence spectra are shown in Figure 2a as a function of the bias voltage. The data reveal that in a relatively narrow window of bias voltage from 2 to 2.8 V the spectra show a rather broad peak (FWHM $\sim$ 200 meV; see Figure 2b), characteristic of plasmonic emission. Contrary to simple metal systems, however, the voltage threshold for emission is shifted by about 0.3 V to higher voltages compared to the expected quantum cutoff condition ($\hbar\omega_{max} = eV_B$ white line in Figure 2a). The intensity of the plasmonic peak decreases very rapidly for voltages larger than 2.8 V, and basically disappears for 3 V. For higher voltages a new set of luminescence peaks appear, consisting of an intense peak at about 1.83 eV, and several side bands at lower photon energies, which are very similar to those reported for C_{60} nanocrystals on 3 ML NaCl/Au(111).[17,18] The new peaks are much narrower than the plasmonic resonance (FWHM $\sim$ 15 meV; see Figure 2b), suggesting an excitonic origin. They can be
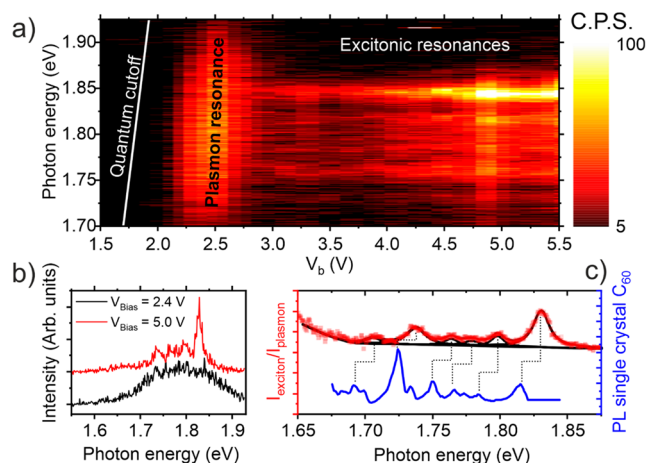
Figure 2. (a) Dependence of the electroluminescence spectra with the applied bias voltage for a tunnel current of 600 pA. The transition from a purely plasmonic to a purely excitonic spectrum is clearly visible between 2.8 and 3 V. The expected quantum cutoff line is marked in white. (b) Examples of individual spectra recorded at tunneling conditions where only the plasmonic or only the excitonic emission is observed. (c) Comparison between the average electroluminescence spectrum at every voltage above 3 V (red dots) and the photoluminescence of defect-free bulk C_{60} crystals[22] (blue line). Black lines are Lorentzian fits to the average, normalized spectrum.

found in the same energy range as that of the plasmonic resonances due to the Purcell effect, which enhances the spontaneous emission rate by a factor proportional to the optical density of states. Indeed, by taking the average of all the spectra recorded for voltages between 3 and 5.5 eV and normalizing to the intensity of the plasmon (to take the Purcell

enhancement into consideration), the resulting spectrum can be fitted by Lorentzian curves revealing all the features observed in photoluminescence of C_{60} crystals[22] (see Figure 2c), with only a typical shift of about 25 meV to higher photon energies. The shift depends on the orientation of the molecule in which the current is injected and on the size of the crystallite and, thus, seems to arise from the effect of the local environment of the molecule under consideration. Notice that PL experiments with negatively charged C_{60} molecules in electrochemical solution reveal the excitonic peaks in the near-infrared, at 1.1 eV.[26] This analysis demonstrates that the electroluminescence spectra in this range of bias voltages originates from the recombination of the same excitons observed in bulk C_{60} crystals.

To compare our results on the voltage dependence of the electroluminescence spectra with the rate of inelastic events, which can be retrieved from the $I(V)$ curves,[21,27] it should be noted that any inelastic event relevant for the processes considered here can only take place while the electron tunnels from the tip to the molecules at the surface of the crystallite, with a voltage difference of just $(1 - \alpha)V_B$ (see Figure 1d). Indeed, direct tunneling from the tip to the Ag surface underneath must be a rare event because the distance between the tip and the Ag surface is about 2.5 nm (the thickness of 2 ML of C_{60} plus 2 ML of NaCl) larger than between the tip and the surface of the molecule. As shown in the Supporting Information, the total rate at which such excitation of energy $\hbar\omega$ can be created by tunneling electrons with a total applied voltage V_B can be calculated by adding all the possible processes marked in blue in Figure 3a and, thus, must be proportional to
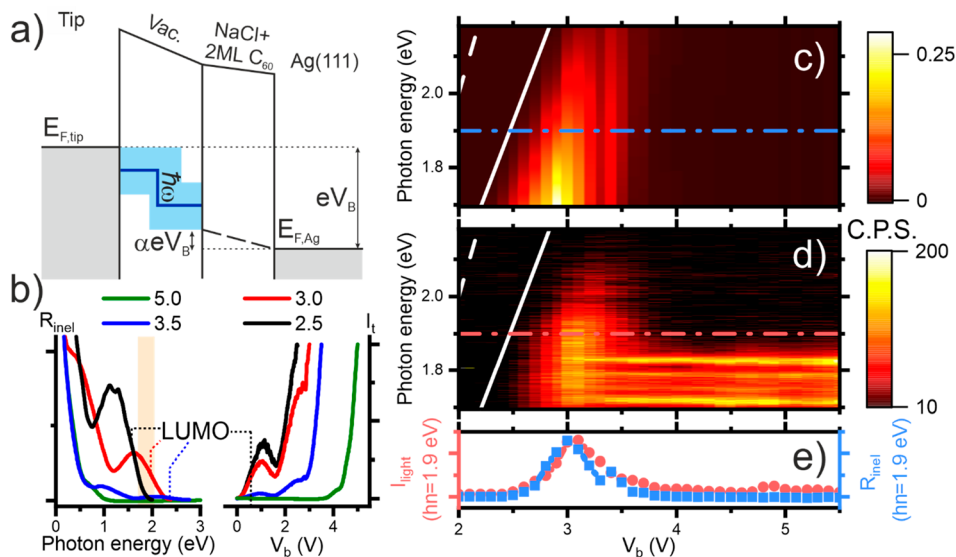
Figure 3. (a) Schematic representation of the inelastic processes that can contribute to the excitation of a photon with energy $\hbar\omega$ in the presence of a dielectric spacer. (b) Experimental rate of inelastic excitations (left panel) obtained from the $I(V)$ curves (right panel) for different stabilization bias voltages. The orange area corresponds to the photon energy range studied in our experiments. (c) Rate of inelastic excitation (linear color scale) for bias voltages between 2 and 5.5 V and photon energies 1.7 and 2.2 eV. The dashed line corresponds to the quantum cutoff condition without considering the dielectric layer, and the solid line corresponds to the correct quantum cutoff condition as determined by eq 3 by the condition $R_{inel}(\hbar\omega, V_B) = 0$. (d) Electroluminescence signal (linear color scale) in the same photon energy and stabilization bias ranges than (c). Both quantum cutoffs are also shown with the same meaning than in (c). (e) Comparison between the inelastic rate and electroluminescence profiles at $\hbar\omega = 1.9$ eV for different bias voltages. The profiles are also marked in (c) and (d) by the blue (rate) and pink (electroluminescence) horizontal dash-dotted lines. In all the panels of this figure a tunnel current of 350 pA has been used.
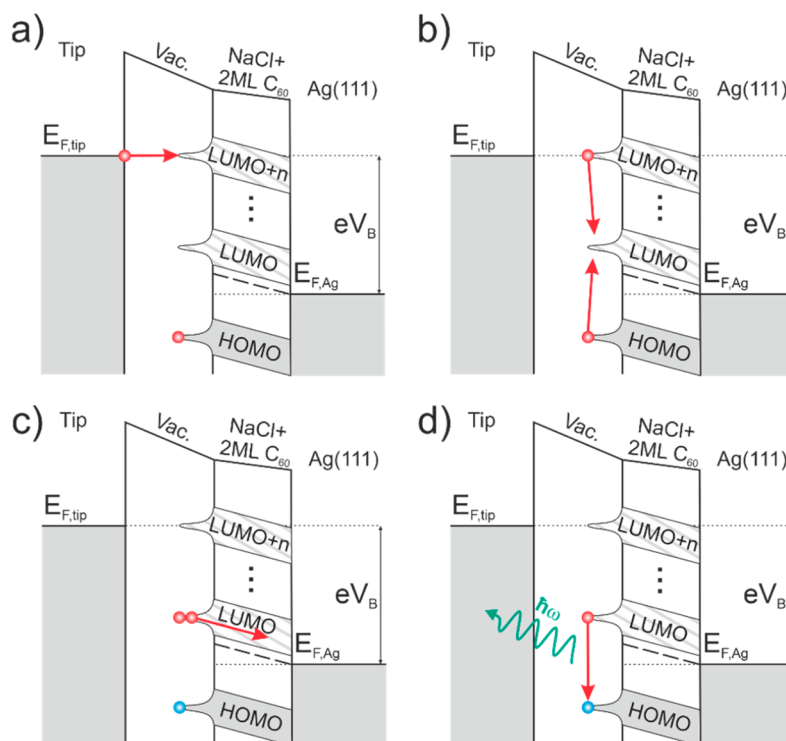
Figure 4. Proposed hot electron mechanism for excitonic tunnel electroluminescence. (a) Initially an elastic tunnel event creates a hot electron in a high energy state, while the electron population of the remaining levels does not change. (b) This hot electron will relax by scattering with other electrons in the occupied bands of the C_{60} nanocrystal. If the energy of the hot electron is at least the energy of the LUMO level plus the exciton energy, then a relaxation in which the hot electron relaxes to the LUMO and an exciton is created becomes possible. (c) The electron diffuses away from the excited C60 molecules, leaving a neutral exciton indistinguishable from those created by optical excitations. (d) The exciton decays radiatively through the emission of a photon.

$$R_{inel}(\hbar\omega, V_B) \propto \int_0^{(1-\alpha)eV_B+\hbar\omega} dE\, \rho_T((1-\alpha)eV_B + \hbar\omega)$$
$$\rho_S(E)T(E, V_B, \hbar\omega) \tag{1}$$

In this expression ρ_T and ρ_S are the densities of electronic states of tip and sample respectively, and T is the transmission factor. On the other hand, a similar argument can be used to obtain the elastic tunnel current that flows between the tip and the sample, yielding the same expression with $\hbar\omega = 0$.

$$I_t(V_B) \propto \int_0^{(1-\alpha)eV_B} dE\, \rho_T(E - (1-\alpha)eV_B)\rho_S(E)T(E, V_B) \tag{2}$$

The remarkable similarity between eqs 1 and 2 can be exploited to evaluate $R_{inel}(\hbar\omega, V_B)$ from the experimentally obtained $I(V)$ curves, yielding

$$R_{inel}(\hbar\omega, V_B) = I_t\left(V_B - \frac{\hbar\omega}{e(1-\alpha)}\right) \tag{3}$$

valid for $\hbar\omega < (1 - \alpha)eV_B$. Equation 3 only differs from our previous analysis for purely metallic tunnel junctions[21] in the $(1 - \alpha)^{-1}$ factor of the photon energy because only a fraction $(1 - \alpha)$ of the applied voltage between the Ag substrate and the tip can be invested in exciting photons. Thus, by recording the $I(V)$ curves at different stabilization voltages and applying eq 3, we can obtain an experimental estimation of the rate at which inelastic transitions occur.

Figure 3b shows the application of this procedure for different stabilization voltages. The right-hand panel of Figure 3b displays the $I(V)$ curves. The onset of conductivity associated with the LUMO and LUMO+1 orbitals at 0.7 and 2.1 V, respectively, can be clearly seen in all the curves (except for the one with a stabilization voltage of 5.0 V). With increasing stabilization voltages, the tip retracts to maintain the current set point constant. The contribution of LUMO and LUMO+1 orbitals to the tunneling current decreases with increasing stabilization voltage because the current now becomes dominated by high-energy electronic states with large vacuum decay lengths, until it becomes negligible for stabilization voltages larger than about 3.5 V.

By applying eq 3, we can obtain the rate of inelastic events as a function of the excitation energy as shown in the left panel of Figure 3b, using our previous estimation $\alpha \approx 0.23$. The general shape of the curves is now reverted in the energy axis, and the zero-rate value corresponds to the excitation energy $\hbar\omega = (1 - \alpha)eV_B$, which becomes the new quantum cutoff condition. The window of photon energies that we explore by tunnel electroluminescence corresponds to the orange-marked area. For stabilization voltages below 2.5 V, the rates are low in this energy window because the contribution of the LUMO orbitals covers a lower range of photon energies. Between 2.5 and 3.5 V, this contribution does overlap with the observed window of photon energies, and thus, we expect a relatively high contribution of inelastic events to the electroluminescence spectra, with electrons starting at tip states and finishing at the LUMO orbital of the C_{60} molecules. For even higher voltages, however, the suppression of the contribution of LUMO and LUMO+1 orbitals to the total current leads to a rather strong

decrease in the rate of inelastic excitations in the explored photon energy window.

Figure 3c collects all the rate curves measured for stabilization voltages between 2 and 5.5 V in the range of photon energies explored in the electroluminescence spectra. The (wrong) $\hbar\omega = eV_B$ cutoff condition is marked with a dashed line, while our new expected cutoff taking the dielectric film under consideration, $\hbar\omega = (1-\alpha)eV_B$, appears as a solid white line. A significant contribution of inelastic tunnel events is thus expected in the region bounded by the cutoff line and the high-bias suppression at about 3.5 V. We compare this expectation with simultaneously recorded electroluminescence spectra in Figure 3d. Notice that since we are using a different tip, the details of plasmonic resonance are somewhat different, but the general phenomenology agrees well with that reported in Figure 2a. Comparison of Figure 3d with Figure 3c, and between the spectral profiles for specific photon energies in Figure 3e, reveals that the plasmonic resonance appears in the range of stabilization voltages and photon energies in which the rate of inelastic transitions is large, as expected since the excitation of the plasmonic luminescence is induced by inelastic tunneling. On the contrary, excitonic peaks appear in the region in which the rate of inelastic transitions is negligible. The creation of excitons, thus, is not related to inelastic tunneling and must be originated by another process that takes place after injection of the hot electron in the C_{60} molecule.

The excitation of molecular luminescence deserves further discussion. As mentioned above, excitonic creation induced by a tunnel current has previously been attributed by some authors to inelastic tunneling events.[5−7,10,13] Our results demonstrate that at least for our system this mechanism is not the one responsible for molecular luminescence. The alternative explanation found in the literature is that the shift in the molecular orbitals due to the dielectric layer pushes the HOMO level above the Fermi level of the metal substrate, thereby enabling the tunnel of an electron away from the HOMO.[4,14,15] However, such a mechanism does not match our experimental observations either. The LUMO level is only 0.6−0.7 eV above the Fermi level, and even if the HOMO level would rise above the Fermi level of the sample in the voltage range explored in our investigations, its separation to the LUMO level would be at most 0.7 eV, too small compared with the exciton energy of 1.83 eV that we observe from the C_{60}. Other processes involving the injection of electrons into the LUMO+1 or higher molecular orbitals followed by a recombination with holes in the LUMO, a hypothetical emptied HOMO level, or other final state alternatives should lead to very different luminescence spectra than that recorded on bulk C_{60} crystals (similar to our observations according to Figure 2c) where the luminescence was explained as a HOMO−LUMO transition facilitated by the Herzberg−Teller effect.[22]

On the basis of our data and the preceding discussion, we propose the following mechanism to explain our observation of excitonic emission induced by tunnel currents. A hot electron produced after elastic tunnel injection (Figure 4a) in a narrow unoccupied band higher than the LUMO, which can be of molecular origin or associated with field emission resonances, can relax to a lower-lying unoccupied band by scattering processes that promote electrons from the (also narrow) occupied bands originated from the HOMO and lower molecular orbitals to empty electronic states. The minimum

transition energy corresponds to the difference between the LUMO and the HOMO energies, minus the electron−hole binding energy (which for C_{60} crystallites can be as high as 1.6 eV[25]) that is, by definition, the exciton energy. Thus, provided that the energy of the hot electron is at least the exciton energy plus the LUMO level, it can relax to the LUMO via creation of an exciton (see Figure 4b). If the exciton lifetime is larger than the inverse of the hopping rate of the hot electron, it will diffuse away before exciton recombination (Figure 4c), which can be facilitated by hybridization of the molecular orbitals with a field emission resonance found at 3.2 eV at the NaCl surface (but not on top of the C_{60} islands).[28,29] Thus, when the exciton recombination finally takes place, it will only reflect the character of the neutral exciton (Figure 4d), explaining the similarity between our data and that of photoluminescence in bulk C_{60} crystals. These considerations also allow for an estimation of the bias threshold to excitonic emission, which should satisfy $eV_{B,th} = \alpha eV_{B,th} + E_{LUMO} + E_{exciton}$, or

$$eV_{B,th} = \frac{E_{LUMO} + E_{exciton}}{1-\alpha} \approx 3 \text{ eV}$$

This estimation is in good qualitative agreement with the data in Figures 2a and 3d, although some excitonic emission can also be observed at some 0.2 V lower bias voltages, an effect that we attribute to the broadening of the LUMO orbital (the onset of which can be estimated at around 0.3 eV, as can be seen in Figure 1c).

To conclude, our systematic study of the dependence of electroluminescence and inelastic rates with the applied bias voltage of C_{60} nanocrystallites on 2 ML of NaCl/Ag(111) has demonstrated that the mechanisms for plasmonic and excitonic radiation are radically different: whereas inelastic tunnel events induce the former process, the latter originates from excitons which are created by relaxation of hot electrons injected at high energies. The difference in the excitation mechanisms enables us to choose our tunneling parameters to promote one of either at will, thereby interrogating only the plasmonic or only the excitonic modes of a QE+cavity system. These results thus open new scenarios to understand molecular electroluminescence processes and can be exploited to design new color-tunable, nanoscale light sources.

■ ASSOCIATED CONTENT

Ⓢⓘ Supporting Information

The Supporting Information is available free of charge at https://pubs.acs.org/doi/10.1021/acs.nanolett.2c02758.

> Methods: sample and tip preparation and data acquisition details; effect of the dielectric layer on the tunneling characteristic curves; occupied electronic states; derivation of eqs 1 and 2 (PDF)

■ AUTHOR INFORMATION

Corresponding Author

Roberto Otero − *IMDEA-Nanoscience Center, 28049 Madrid, Spain; Departamento de Física de la Materia Condensada & IFIMAC, Universidad Autónoma de Madrid, 28049 Madrid, Spain;* ⓞ orcid.org/0000-0001-6936-4003; Email: roberto.otero@uam.es

Authors

Alberto Martín-Jiménez − *IMDEA-Nanoscience Center, 28049 Madrid, Spain*

Óscar Jover − *IMDEA-Nanoscience Center, 28049 Madrid, Spain; Departamento de Física de la Materia Condensada & IFIMAC, Universidad Autónoma de Madrid, 28049 Madrid, Spain*

Koen Lauwaet − *IMDEA-Nanoscience Center, 28049 Madrid, Spain*

Daniel Granados − *IMDEA-Nanoscience Center, 28049 Madrid, Spain;* orcid.org/0000-0001-7708-9080

Rodolfo Miranda − *IMDEA-Nanoscience Center, 28049 Madrid, Spain; Departamento de Física de la Materia Condensada & IFIMAC, Universidad Autónoma de Madrid, 28049 Madrid, Spain*

Complete contact information is available at:
https://pubs.acs.org/10.1021/acs.nanolett.2c02758

Author Contributions

The experiments were performed by A.M.-J., O.J., and K.L. The experimental setup was designed by K.L. and D.G. Data analysis was performed by R.O. and K.L., and the interpretation was a contribution of R.O. and R.M. The manuscript was written through contributions of all authors. All authors have given approval to the final version of the manuscript.

Notes

The authors declare no competing financial interest.

■ REFERENCES

(1) Agarwal, G. S.*Quantum Optics*; Cambridge University Press: 2013.

(2) Gerry, C.; Knight, P.*Introductory Quantum Optics*; Cambridge University Press: 2005.

(3) Chikkaraddy, R.; de Nijs, B.; Benz, F.; Barrow, S. J.; Scherman, O. A.; Rosta, E.; Demetriadou, A.; Fox, P.; Hess, O.; Baumberg, J. J. Single-Molecule Strong Coupling at Room Temperature in Plasmonic Nanocavities. *Nature* 2016, 535 (7610), 127−130.

(4) Kuhnke, K.; Große, C.; Merino, P.; Kern, K. Atomic-Scale Imaging and Spectroscopy of Electroluminescence at Molecular Interfaces. *Chem. Rev.* 2017, 117 (7), 5174−5222.

(5) Doppagne, B.; Chong, M. C.; Bulou, H.; Boeglin, A.; Scheurer, F.; Schull, G. Electrofluorochromism at the Single-Molecule Level. *Science* 2018, 361 (6399), 251−255.

(6) Rai, V.; Gerhard, L.; Sun, Q.; Holzer, C.; Repän, T.; Krstić, M.; Yang, L.; Wegener, M.; Rockstuhl, C.; Wulfhekel, W. Boosting Light Emission from Single Hydrogen Phthalocyanine Molecules by Charging. *Nano Lett.* 2020, 20 (10), 7600−7605.

(7) Hung, T. C.; Kiraly, B.; Strik, J. H.; Khajetoorians, A. A.; Wegner, D. Plasmon-Driven Motion of an Individual Molecule. *Nano Lett.* 2021, 21 (12), 5006−5012.

(8) Doležal, J.; Canola, S.; Merino, P.; Švec, M. Exciton-Trion Conversion Dynamics in a Single Molecule. *ACS Nano* 2021, 15 (4), 7694−7699.

(9) Imada, H.; Miwa, K.; Imai-Imada, M.; Kawahara, S.; Kimura, K.; Kim, Y. Single-Molecule Investigation of Energy Dynamics in a Coupled Plasmon-Exciton System. *Phys. Rev. Lett.* 2017, 119 (1), 013901.

(10) Chen, G.; Luo, Y.; Gao, H.; Jiang, J.; Yu, Y.; Zhang, L.; Zhang, Y.; Li, X.; Zhang, Z.; Dong, Z. Spin-Triplet-Mediated Up-Conversion and Crossover Behavior in Single-Molecule Electroluminescence. *Phys. Rev. Lett.* 2019, 122 (17), 177401.

(11) Luo, Y.; Chen, G.; Zhang, Y.; Zhang, L.; Yu, Y.; Kong, F.; Tian, X.; Zhang, Y.; Shan, C.; Luo, Y.; Yang, J.; Sandoghdar, V.; Dong, Z.; Hou, J. G. Electrically Driven Single-Photon Superradiance from Molecular Chains in a Plasmonic Nanocavity. *Phys. Rev. Lett.* 2019, 122 (23), 233901.

(12) Gutzler, R.; Garg, M.; Ast, C. R.; Kuhnke, K.; Kern, K. Light-Matter Interaction at Atomic Scales. *Nat. Rev. Phys. 2021 3:6* 2021, 3 (6), 441−453.

(13) Kröger, J.; Doppagne, B.; Scheurer, F.; Schull, G. Fano Description of Single-Hydrocarbon Fluorescence Excited by a Scanning Tunneling Microscope. *Nano Lett.* 2018, 18 (6), 3407−3413.

(14) Merino, P.; Rosławska, A.; Große, C.; Leon, C. C.; Kuhnke, K.; Kern, K. Bimodal Exciton-Plasmon Light Sources Controlled by Local Charge Carrier Injection. *Sci. Adv.* 2018, 4 (5), eaap834.

(15) Qiu, X. H.; Nazin, G. v.; Ho, W. Vibrationally Resolved Fluorescence Excited with Submolecular Precision. *Science* 2003, 299 (5606), 542−546.

(16) Rossel, F.; Pivetta, M.; Schneider, W.-D. Luminescence Experiments on Supported Molecules with the Scanning Tunneling Microscope. *Surf. Sci. Rep.* 2010, 65 (5), 129−144.

(17) Rossel, F.; Pivetta, M.; Patthey, F.; Schneider, W.-D. Plasmon Enhanced Luminescence from Fullerene Molecules Excited by Local Electron Tunneling. *Opt. Express* 2009, 17 (4), 2714−2721.

(18) Ćavar, E.; Blüm, M. C.; Pivetta, M.; Patthey, F.; Chergui, M.; Schneider, W. D. Fluorescence and Phosphorescence from Individual C60 Molecules Excited by Local Electron Tunneling. *Phys. Rev. Lett.* 2005, 95 (19), 196102.

(19) Persson, B. N. J.; Baratoff, A. Inelastic Electron Tunneling from a Metal Tip: The Contribution from Resonant Processes. *Phys. Rev. Lett.* 1987, 59 (3), 339−342.

(20) Berndt, R.; Gimzewski, J. K.; Johansson, P. Inelastic Tunneling Excitation of Tip-Induced Plasmon Modes on Noble-Metal Surfaces. *Phys. Rev. Lett.* 1991, 67 (27), 3796.

(21) Martín-Jiménez, A.; Fernández-Domínguez, A. I.; Lauwaet, K.; Granados, D.; Miranda, R.; García-Vidal, F. J.; Otero, R. Unveiling the Radiative Local Density of Optical States of a Plasmonic Nanocavity by STM. *Nat. Commun.* 2020, 11 (1), 1021.

(22) Akimoto, I.; Kan'no, K. I. Photoluminescence and Near-Edge Optical Absorption in the Low-Temperature Phase of Pristine C60 Single Crystals. *J. Phys. Soc. Jpn.* 2002, 71 (2), 630−643.

(23) Rossel, F.; Pivetta, M.; Patthey, F.; Ćavar, E.; Seitsonen, A. P.; Schneider, W. D. Growth and Characterization of Fullerene Nanocrystals on NaCl/Au(111). *Phys. Rev. B* 2011, 84 (7), 075426.

(24) Imai-Imada, M.; Imada, H.; Miwa, K.; Jung, J.; Shimizu, T. K.; Kawai, M.; Kim, Y. Energy-Level Alignment of a Single Molecule on Ultrathin Insulating Film. *Phys. Rev. B* 2018, 98 (20), 201403.

(25) Lof, R.W.; van Veenendaal, M.A.; Jonkman, H.T.; Sawatzky, G.A. Band Gap, Excitons, and Coulomb Interaction in Solid C60. *J. Electron Spectrosc. Relat. Phenom.* 1995, 72, 83−87.

(26) Kato, T. Absorption and Emission Spectra for C60 Anions. *Laser Chem.* 1994, 14, 155−160.

(27) Martín-Jiménez, A.; Lauwaet, K.; Jover, Ó.; Granados, D.; Arnau, A.; Silkin, V. M.; Miranda, R.; Otero, R. Electronic Temperature and Two-Electron Processes in Overbias Plasmonic Emission from Tunnel Junctions. *Nano Lett.* 2021, 21 (16), 7086−7092.

(28) Ploigt, H.-C.; Brun, C.; Pivetta, M.; Patthey, F.; Schneider, W.-D. Local work function changes determined by field emission resonances: NaCl/Ag(100). *Phys. Rev. B* **2007**, *76*, 195404.

(29) Borca, B.; Barja, S.; Garnica, M.; Sánchez-Portal, D.; Silkin, V. M.; Chulkov, E. V.; Hermanns, C. F.; Hinarejos, J. J.; Vázquez de Parga, A. L.; Arnau, A.; Echenique, P. M.; Miranda, R. Potential Energy Landscape for Hot Electrons in Periodically Nanostructured Graphene. *Phys. Rev. Lett.* **2010**, *105*, 036804.